Redox Biology 40 (2021) 101859

Contents lists available at ScienceDirect

Redox Biology

journal homepage: www.elsevier.com/locate/redox

The protective effects of fibroblast growth factor 10 against hepatic ischemia-reperfusion injury in mice

Santie Li [a,b,1], Zhongxin Zhu [a,1], Mei Xue [c,1], Xuebo Pan [a,1], Gaozan Tong [a], Xinchu Yi [a], Junfu Fan [a], Yuankuan Li [a], Wanqian Li [a], Yetong Dong [a], Enzhao Shen [a], Wenjie Gong [a], Xuejiao Wang [a], Ying Yu [a], Yoo Jae Maeng [a], Xiaokun Li [a], Kwang Youl Lee [b,**], Litai Jin [a,***], Weitao Cong [a,*]

[a] School of Pharmaceutical Science, Wenzhou Medical University, Wenzhou, PR China
[b] College of Pharmacy and Research Institute of Drug Development, Chonnam National University, Gwangju, Republic of Korea
[c] Central Laboratory, The First Affiliated Hospital of Wenzhou Medical University, Wenzhou, PR China

ARTICLE INFO

Keywords:
Apoptosis
Inflammatory response
Liver regeneration
Reactive oxygen species
Nuclear factor-erythroid 2-related factor 2

ABSTRACT

Hepatic ischemia-reperfusion injury (IRI) is a major complication of liver surgery and transplantation. IRI leads to hepatic parenchymal cell death, resulting in liver failure, and lacks effective therapeutic approaches. Fibroblast growth factor 10 (FGF10) is a paracrine factor which is well-characterized with respect to its pro-proliferative effects during embryonic liver development and liver regeneration, but its role in hepatic IRI remains unknown. In this study, we investigated the role of FGF10 in liver IRI and identified signaling pathways regulated by FGF10. In a mouse model of warm liver IRI, FGF10 was highly expressed during the reperfusion phase. *In vitro* experiments demonstrated that FGF10 was primarily secreted by hepatic stellate cells and acted on hepatocytes. The role of FGF10 in liver IRI was further examined using adeno-associated virus-mediated gene silencing and overexpression. Overexpression of FGF10 alleviated liver dysfunction, reduced necrosis and inflammation, and protected hepatocytes from apoptosis in the early acute injury phase of IRI. Furthermore, in the late phase of IRI, FGF10 overexpression also promoted hepatocyte proliferation. Meanwhile, gene silencing of FGF10 had the opposite effect. Further studies revealed that overexpression of FGF10 activated nuclear factor-erythroid 2-related factor 2 (NRF2) and decreased oxidative stress, mainly through activation of the phosphatidylinositol-3-kinase/AKT pathway, and the protective effects of FGF10 overexpression were largely abrogated in NRF2 knockout mice. These results demonstrate the protective effects of FGF10 in liver IRI, and reveal the important role of NRF2 in FGF10-mediated hepatic protection during IRI.

1. Introduction

Ischemia-reperfusion injury (IRI) in the liver remains a serious clinical complication that can occur during liver trauma, liver resection or transplantation, and hemorrhagic shock [1,2]. IRI induces hepatic histopathological changes, and is the main cause of liver failure and dysfunction after surgery [1–3]. Hepatic IRI can be divided into the early acute injury phase and the later recovery phase, and the mechanisms underlying the two processes are complex [4,5]. For example, at the early stage of reperfusion (the injury phase), overproduction of reactive oxygen species (ROS) can upset the natural redox balance, inducing redox-regulated signaling pathways, such as the c-Jun N-terminal kinase 1/2 (JNK1/2) and nuclear factor-κB (NF-κB) pathways, resulting in apoptosis and inflammation [4,6,7]. Afterward, at the late stage of reperfusion (the recovery phase), the liver undergoes enhanced regeneration, which is associated with hepatocyte growth and proliferation [4,5]. Both of the two phases are important for the restoration of liver function after IRI.

The fibroblast growth factor (FGF) family consists of 22 members, most of which play key roles in organ development, repair, metabolism, and homeostasis [8]. Among them, FGF10 belongs to the FGF7

* Corresponding author.
** Corresponding author.
*** Corresponding author.
E-mail addresses: kwanglee@chonnam.ac.kr (K.Y. Lee), jin_litai@126.com (L. Jin), cwt97126@126.com (W. Cong).
[1] Co-first authors.

https://doi.org/10.1016/j.redox.2021.101859
Received 14 December 2020; Received in revised form 2 January 2021; Accepted 4 January 2021
Available online 7 January 2021

List of abbreviations

AAV	adeno-associated virus
ALT	alanine aminotransferase
AST	aspartate aminotransferase
Bcl-2	B-cell lymphoma 2
c-CAS-3	cleaved caspase 3
CD68	cluster of differentiation 68
DCFH-DA	2′,7′-dichlorofluorescin diacetate
DHE	dihydroethidium
ERK	extracellular-signal-regulated kinase
FGF10	fibroblast growth factor 10
FGFR	fibroblast growth factor receptor
FoxO	forkhead box O
FRS2α	FGFR substrate 2-α
GSK3β	glycogen synthase kinase 3β
H&E	hematoxylin and eosin
H/R	hypoxia-reoxygenation
HSCs	hepatic stellate cells
IκBα	inhibitory κB α
IL	interleukin
IRI	ischemia-reperfusion injury
IHC	immunohistochemistry
JNK1/2	c-Jun N-terminal kinase 1/2
KEAP1	kelch-like ECH-associated protein 1
KO	knockout
LPO	lipid peroxidation
MAPK	mitogen-activated protein kinase
MEK	MAPK/ERK kinase
MPO	myeloperoxidase
NAC	N-acetyl-L-cysteine
NF-κB	nuclear factor-κB
NQO-1	NAD(P)H dehydrogenase [quinone] 1
NRF2	nuclear factor-erythroid 2-related factor 2
PCNA	proliferating cell nuclear antigen
PI3K	phosphatidylinositol-3-kinase
ROS	reactive oxygen species
α-SMA	α-smooth muscle actin
TNF-α	tumor necrosis factor-α
TUNEL	terminal deoxynucleotidyl transferase-mediated dUTP nick end labelling

subfamily and is a well-known mesenchymal-epithelial signaling growth factor through binding to fibroblast growth factor receptors (FGFRs) [9]. FGF10 binds to FGFR2b (the epithelial splice form of FGFR2) with high affinity, and its downstream signaling is also mediated through FGFR2b [10]. There have also been reports demonstrating that FGF10 can bind to FGFR1b (the epithelial splice form of FGFR1), but with much lower affinity [11]. FGF10 plays essential roles in limb, lung, kidney, salivary gland, and adipose tissue development [10,12], as well as in the liver [13]. During embryonic liver development, FGF10-FGFR2b signaling and the downstream β-catenin activation controls liver size and hepatoblast survival, and knockdown of FGF10 or FGFR2b significantly reduces hepatoblast proliferation and therefore liver size [13]. In adult mice, FGF10 overexpression increases the expansion of hepatic progenitor cells and can promote liver regeneration after partial hepatectomy [14]. However, the role of FGF10 in hepatic IRI is unknown.

The phosphatidylinositol-3-kinase (PI3K)/AKT and RAS/mitogen-activated protein kinase (MAPK) pathways are well known to be regulated by FGF10 [10,12]. Interestingly, FGF10-regulated PI3K/AKT signaling controls β-catenin activation, which affects liver size during embryonic development [13], and the ability of FGF10 to regulate liver regeneration in adult mice is also PI3K/AKT-dependent [14]. The PI3K/AKT pathway is considered to be a pro-survival pathway which can regulate cell growth, proliferation, differentiation, migration, and metabolism in the context of many diseases [15,16]. There is also growing evidence shows that AKT activation may protect against hepatic IRI [2,3,17]. AKT signaling suppresses apoptosis and inflammatory responses, thus improving hepatocyte viability [3]. It can affect a large number of downstream effectors, including B-cell lymphoma 2 (Bcl-2), cleaved caspase 3 (c-CAS-3), forkhead box O (FoxO), p38 MAPK, JNK1/2, and NF-κB [3,16], and is associated with many protective processes in liver IRI [2,3,17,18].

The nuclear factor-erythroid 2-related factor 2 (NRF2) is a master regulator of redox homeostasis in many liver diseases, including IRI [17,19]. NRF2 is a transcription factor which can regulate the expression of antioxidants, enzymes involved in metabolism and detoxification, transporters, and autophagy-related proteins [17,20]. Previous studies demonstrate that kelch-like ECH-associated protein 1 (KEAP1) is an important regulator of NRF2 expression, KEAP1 acts as a repressor of NRF2, as binding of KEAP1 to NRF2 results in its ubiquitination and degradation [20]. Interestingly, KEAP1 expression has been shown to be regulated by FoxO3 [21], while FoxO3 is inactivated by AKT activation [16], indicating that PI3K/AKT signaling can regulate NRF2 activation. In addition, studies have also demonstrated that PI3K/AKT signaling can control NRF2 nuclear export and degradation [22]. In the present study, we show that overexpression of FGF10 protects against liver IRI by decreasing apoptosis, inflammation, oxidative stress, and promoting hepatocyte proliferation. Mechanically, we observed the protective effects of FGF10 overexpression are largely dependent on PI3K/AKT-mediated NRF2 activation. The results of our study unveil a new role of FGF10 in the regulation of hepatic IRI.

2. Materials and methods

2.1. Animals

Male C57BL/6 mice and NRF2 knockout mice (C57BL/6 background as previously described [19]) at the age of 8- to 10-week-old were used in this study. Mice were housed in temperature-controlled pathogen-free facility with 12-h light/dark cycle and had access to food and water *ad libitum*. Animals received human care according to the "Guide for the Care and Use of Laboratory Animals" prepared by the National Academy of Sciences and published by the National Institutes of Health (NIH publication 86-23 revised 1985). All animal procedures were approved by the Institutional Animal Care and Use Committee of Wenzhou Medical University.

For studies in FGF10 overexpression or knockdown, each C57BL/6 mice was intravenously injected with a single dose of 1×10^{11} vector genomes of adeno-associated virus (AAV) serotype 9 carrying either *Fgf10* (AAV-*Fgf10*), *Fgf10*-interfering sequence (AAV-sh-*Fgf10*), *GFP* control gene (AAV-*GFP*) or control-interfering sequence (AAV-sh-Con) with the CMV promoter (All of which contain the GFP tag). For well transfection, three weeks later after the injection, mice were started to use for further experiments. NRF2 knockout mice with AAV transfection were under the same procedure. AAV-*GFP*, AAV-sh-Con, AAV-*Fgf10* (contract number: HYSW-BD-PTHC-2018100004) and AAV-sh-*Fgf10* (contrast number: HYSW-BD-YZKC-2018040052) were constructed and purchased from OBiO Technology (Shanghai) Corp., Ltd.

For *in vivo* AKT inhibition, mice were i.p. injected with saline or PI3K inhibitor LY294002 (2.5 mg/kg; Selleck) 1 h prior to liver IRI.

2.2. Mouse warm hepatic IRI model

As previously described [6], a well-established partial (70%) liver warm ischemia mouse model was used in our research. Briefly, mice were first anesthetized by pentobarbital sodium (60 mg/kg; Sigma), then a midline laparotomy was performed, and a microvascular clip was used to clamp the portal vein, hepatic artery, and bile duct to interrupt the blood supply to the left lateral/median lobes of the liver. After 90 min of ischemia, the clamp was removed to cause reperfusion, and after indicated time points of reperfusion, the animals were sacrificed to collect liver tissues, other organ tissues, and serum samples for further analysis. For sham control group, mice underwent the same surgical procedure but without clamping the portal triad.

2.3. Mouse primary hepatocytes isolation

Primary hepatocytes were isolated according to a previous report [23]. Briefly, 8- to 10-week-old male C57BL/6 mice were anesthetized, and the liver was perfused in situ through the portal vein with Ca^{2+} and Mg^{2+} free Hank's balanced salt solution (HBSS; Gibco) followed by 0.05% collagenase IV (Gibco) solution (diluted in HBSS containing Ca^{2+} and Mg^{2+}). After perfusion, liver was rapidly moved from the body and carefully dispersed into cold HBSS, then the cell suspension was filtered through a 70-μm strainer and the hepatocytes were pelleted three times at 50 g for 4 min. Primary hepatocytes were cultured in high-glucose Dulbecco's modified Eagle's medium (DMEM; Sigma) supplemented with 10% fetal bovine serum (FBS; Sigma) and 1% penicillin/streptomycin (P/S; Gibco) in laminin coated 6-well culture Petri dishes (Corning), and maintained in a humidified incubator with 5% CO_2 at 37 °C.

2.4. Mouse primary hepatic stellate cells isolation

Primary hepatic stellate cells (HSCs) were isolated by pronase and collagenase digestion followed by density gradient centrifugation according to a previous report [24]. Briefly, 24- to 26-week-old male C57BL/6 mice were used, and the liver was first in situ digested by 0.05% pronase E (Sigma) and 0.03% collagenase IV solution, then further digested by pronase E, collagenase IV and DNase I (Sigma) solution at 37 °C shaking for 20 min. Hepatic stellate cells (HSCs) were isolated from the non-parenchymal cell suspension by using the 11.5% and 20% OptiPrep (Axis-Shield) solution at 1400 g for 20 min at 4 °C. HSCs were cultured in high-glucose DMEM containing 10% FBS and 1% P/S in a humidified incubator with 5% CO_2 at 37 °C.

2.5. Cell lines culture

The human normal liver cell line L-02 and the human activated hepatic stellate cell line LX-2 were purchased from Procell Life Science&Technology Co., Ltd. Both the L-02 and LX-2 cells were maintained in high-glucose DMEM containing 10% FBS and 1% P/S in a humidified incubator with 5% CO_2 at 37 °C.

2.6. In vitro hypoxia-reoxygenation (H/R) model

H/R model was performed according to a previous report [25], the cell culture medium was first changed to glucose-free and serum-free DMEM, then the cells were removed to a hypoxia incubator chamber (containing 1% O_2, 5% CO_2, and 94% N_2), after 6 h of hypoxia, cells were returned to normal culture condition (95% air, 5% CO_2) and the medium was replaced to complete DMEM (containing 10% FBS and 1% P/S) for another 6 h to simulate IRI *in vitro*.

For *in vitro* AKT inhibition, primary hepatocytes were pretreated with saline or 50 μM LY294002 for 1 h.

2.7. RNA interference in vitro

For RNA interference, primary hepatocytes were transfected with control scramble siRNA (Santa Cruz Biotechnology), FGFR2 siRNA (Santa Cruz Biotechnology), or FGFR1 siRNA (Santa Cruz Biotechnology), and primary HSCs were transfected with control scramble siRNA or FGF10 siRNA (Santa Cruz Biotechnology). Transfection was started by using the Lipofectamine RNAiMAX Transfection Reagent (Thermo Fisher Scientific) in Opti-MEM (Gibco) for 12 h at first, then the medium was changed to complete DMEM for another 12 h to get ready for further experiments.

2.8. Transwell system

Transwell chamber with 0.4 μm pore size (Corning) was used in this study. Primary hepatocytes were seeded on the bottom of the 6-well plate, and HSCs were cultured onto the membrane of Transwell cell culture inserts. After scramble siRNA or FGF10 siRNA transfection, the Transwell inserts containing the HSCs were placed into the six-well plate containing the hepatocytes to initiate the experiment.

2.9. Histology and immunohistochemistry (IHC)

Hematoxylin and eosin (H&E) staining was used to assess the necrosis area of the liver. Mouse liver tissues were fixed in 10% formalin, embedded in paraffin and sectioned to 5 μm slides. The slides were deparaffinized and stained by a Hematoxylin-Eosin Staining Kit (Solarbio) according to the manufacturer's protocol. For IHC staining, liver sections were subjected to deparaffinization and antigen retrieval at first, then the non-specific antibody binding was blocked by using 10% bovine serum albumin (BSA; Biosharp) at room temperature for 1 h. After incubating with primary antibodies of FGF10 (ABN44, Millipore, 1:1000 dilution), Ki-67 (12202, Cell Signaling Technology, 1:400 dilution), CD68 (sc-20060, Santa Cruz Biotechnology, 1:50 dilution), or MPO (ab9535, Abcam, 1:50 dilution) at 4 °C overnight, appropriate secondary antibodies conjugated with HRP were added and incubated at room temperature. A Metal Enhanced DAB Substrate Kit (Solarbio) was used to visualize the sections followed by hematoxylin counterstaining. All images were captured by using a Nikon ECLIPSE Ni microscope.

2.10. Immunofluorescence

For *in vivo* experiments, fresh frozen AAV transfected mouse liver tissues were sectioned to 5 μM and stained with DAPI (Beyotime) for 10 min. For *in vitro* experiments, primary HSCs were first fixed in 4% paraformaldehyde for 15 min and then permeabilized in 0.5% Triton X-100 for 15 min at room temperature. Cells were then blocked by 5% BSA and incubated with anti-desmin (5332, Cell Signaling Technology, 1:100 dilution) or anti-α-SMA (19245, Cell Signaling Technology, 1:200 dilution) antibodies at 4 °C overnight followed by appropriate secondary antibodies conjugated with Alexa Fluor 647. Finally, the cell nuclei were stained with DAPI. Images were visualized and captured by using a Leica SP8 confocal microscope.

2.11. Terminal deoxynucleotidyl transferase-mediated dUTP nick end labelling (TUNEL) assay

The DeadEnd™ Colorimetric TUNEL System (Promega) was used to detect in situ hepatocyte apoptosis in formalin-fixed paraffin-embedded liver sections followed by the manufacturer's protocol. Images were captured by using a Nikon ECLIPSE Ni microscope.

2.12. Redox state measurements

DHE staining was used to detect ROS production in mouse liver tissues. Unfixed fresh frozen liver sections (10 μm) were immediately

incubated with 5 μM dihydroethidium (Invitrogen) at 37 °C for 15 min. After the incubation, slides were washed with ice-cold PBS for three times and then visualized by using a Leica SP8 confocal microscope. All procedures were protected from light.

Lipid peroxidation (LPO) levels (manifested as MDA production) and the ratio of oxidized/total glutathione (manifested as GSSG/GSH) were determined as indirect measurements of *in vivo* ROS production. Lipid Peroxidation MDA Assay Kit (Beyotime Biotechnology), GSH and GSSG Assay Kit (Beyotime Biotechnology) were used for these detections in liver tissue homogenates according to the manufacturer's protocols.

ROS production *in vitro* was measured by DCFH-DA staining. Primary hepatocytes were incubated with 10 μM 2′,7′-dichlorofluorescin diacetate (Sigma) at 37 °C for 30 min and the fluorescence was visualized by Leica SP8 confocal microscopy. All procedures were protected from light.

2.13. Alanine aminotransferase (ALT) and aspartate aminotransferase (AST) measurements

Serum ALT/AST levels were measured by using the ALT and AST assay kits (Nanjing Jiancheng Bioengineering Institute) according to the manufacturer's protocols.

2.14. Western blot

RIPA lysis buffer (Thermo Fisher Scientific) with Protease and Phosphatase Inhibitor Cocktail (Abcam) was used to extract total proteins from fresh liver tissues and cell samples. Nuclear proteins were isolated by using the Pierce NE-PER nuclear and cytoplasmic extraction kit (Thermo Fisher Scientific). Protein concentrations were detected by using the Pierce BCA Protein Assay Kit (Thermo Fisher Scientific), and proteins were separated by SDS-PAGE and transferred to PVDF membrane (Millipore) followed by blocking with 5% non-fat milk (BD Biosciences). After incubation with primary and secondary antibodies, each blot was developed by using the ECL regent (Millipore) and captured by Amersham Image 600 system (GE Healthcare Life Sciences). Antibodies used in the western blot are listed in Supplementary Table 1.

2.15. Quantitative RT-PCR

TRIzol Reagent (Invitrogen) was used to extract total RNA from cells or fresh frozen liver tissues. Complementary DNA was reverse transcribed by using the GoScript Reverse Transcription System (Promega), and quantitative RT-PCR was performed with SYBR Green PCR Master Mix (Thermo Fisher Scientific) following the manufacturers' protocols. The mRNA levels were normalized to β-actin expression. The primer sequences of the target genes are shown in Supplementary Table 2.

2.16. Statistical analysis

All data in this study were analyzed by GraphPad Prism 7.0 and were expressed as mean ± SD. Two-tailed Student's *t*-test (between two groups) and one-way analysis of variance (between multiple groups) were used for comparisons, and a value of $P < 0.05$ was considered statistically significant.

3. Results

3.1. FGF10 is significantly upregulated during hepatic IRI

To analyze the correlation between FGF10 and hepatic IRI, we first assessed the protein expression of FGF10 at various time points after reperfusion in our mouse model. By western blotting and IHC, we found that FGF10 protein expression was markedly increased in the liver after IRI, and the expression peaked at 6 h post-injury (Fig. 1A and B), indicating that FGF10 was expressed at the early injury phase of IRI. Furthermore, IHC staining revealed that FGF10 was significantly increased in the necrotic areas of the liver (Fig. 1B), suggesting that it might play a pivotal role in the regulation of liver function after IRI.

As a paracrine factor, FGF10 can be secreted by multiple organs [10,12], and hepatic IRI may also influence the systemic metabolism. Therefore, we assessed the protein expression of FGF10 in different organs by western blotting. This analysis demonstrated that the liver was the main site of FGF10 expression after hepatic IRI (Fig. 1C).

FGF10/FGFR2b-mediated mesenchymal-epithelial signaling has been shown to play important roles in various tissues [9–12]. In the liver, studies have suggested that FGF10 is expressed by myofibroblasts/HSCs, and its receptor, FGFR2b, is expressed by hepatocytes [13,26]. Therefore, we isolated mouse primary hepatocytes and HSCs in our study (Supplementary Fig. 1A), and the results indicated that FGF10 was upregulated in primary HSCs after H/R stimulation (Fig. 1D), while FGFR2b was specifically expressed by hepatocytes (Fig. 1E). We also verified the expression of FGF10 and FGFR2b in cell lines (the human normal hepatocytes L-02 and the human activated hepatic stellate cells LX-2), and the results were consist with mouse primary cells (Fig. 1F and G). These experiments preliminarily indicate that HSC-secreted FGF10 mostly acts on hepatocytes during liver IRI.

3.2. ROS mediates the expression of FGF10 in HSCs, while FGF10 acts through FGFR2b on hepatocytes

We next sought to determine how HSC sense IRI and release FGF10. Considering that FGF10 was markedly upregulated at the early injury phase of hepatic IRI, and ROS production is also a key event occurs in this phase [4], together with proofs that ROS play a pivotal role in HSC activation [27–29], we hypothesized that ROS mediated the activation of HSCs and the subsequent releasement of FGF10 during hepatic IRI. To test the hypothesis, we first treated mouse primary HSCs with H_2O_2, and the results indicated that the protein expression of α-SMA (marker of HSC activation) and FGF10 were significantly increased after H_2O_2 treatment (Fig. 2A), meanwhile, immunofluorescence staining of α-SMA also confirmed the result (Supplementary Fig. 2A). We then tested the effect of antioxidant N-acetyl-L-cysteine (NAC) in our H/R model, as shown in Fig. 2B, H/R stimulation increased the protein expression of α-SMA and FGF10 in mouse primary HSCs, while NAC treatment restrained the increase of α-SMA and FGF10 after H/R, together with the results of α-SMA immunofluorescence staining (Supplementary Fig. 2B). These results indicate that ROS lead to HSC activation and FGF10 expression in liver IRI.

As both of FGFR2b and FGFR1b are receptors of FGF10, we wondered which receptor played a dominant role in FGF10's downstream signaling. Accordingly, we used siRNA transfection to knockdown the expression of FGFR2b or FGFR1b in mouse primary hepatocytes (Supplementary Fig. 2C), followed by treatment with mouse recombinant FGF10 (rFGF10) for 1 h (as our results indicated that AKT activation reached a peak at 1 h after rFGF10 treatment; Supplementary Fig. 2D), and the results showed that the levels of phosphorylated FGFR substrate 2-α (FRS2α) and phosphorylated AKT were both increased after rFGF10 treatment, indicating the activation of FGF10 signaling, while FGFR2b knockdown blocked the upregulation of phospho-FRS2α and phospho-AKT (Fig. 2C). In contrast, FGFR1b knockdown did not affect the upregulation of phospho-FRS2α and phospho-AKT induced by rFGF10 (Fig. 2D). Taken together, these results remind us that FGF10 mostly acts through FGFR2b on hepatocytes.

3.3. FGF10 alleviates liver damage and regulates AKT activation during hepatic IRI

To confirm the role of FGF10 in liver IRI, we utilized AAV-mediated gain- and loss-of-function approaches, which resulted in successful FGF10 overexpression and knockdown, respectively (Supplementary Fig. 3A and B). It should be noticed that the AAV transfection caused

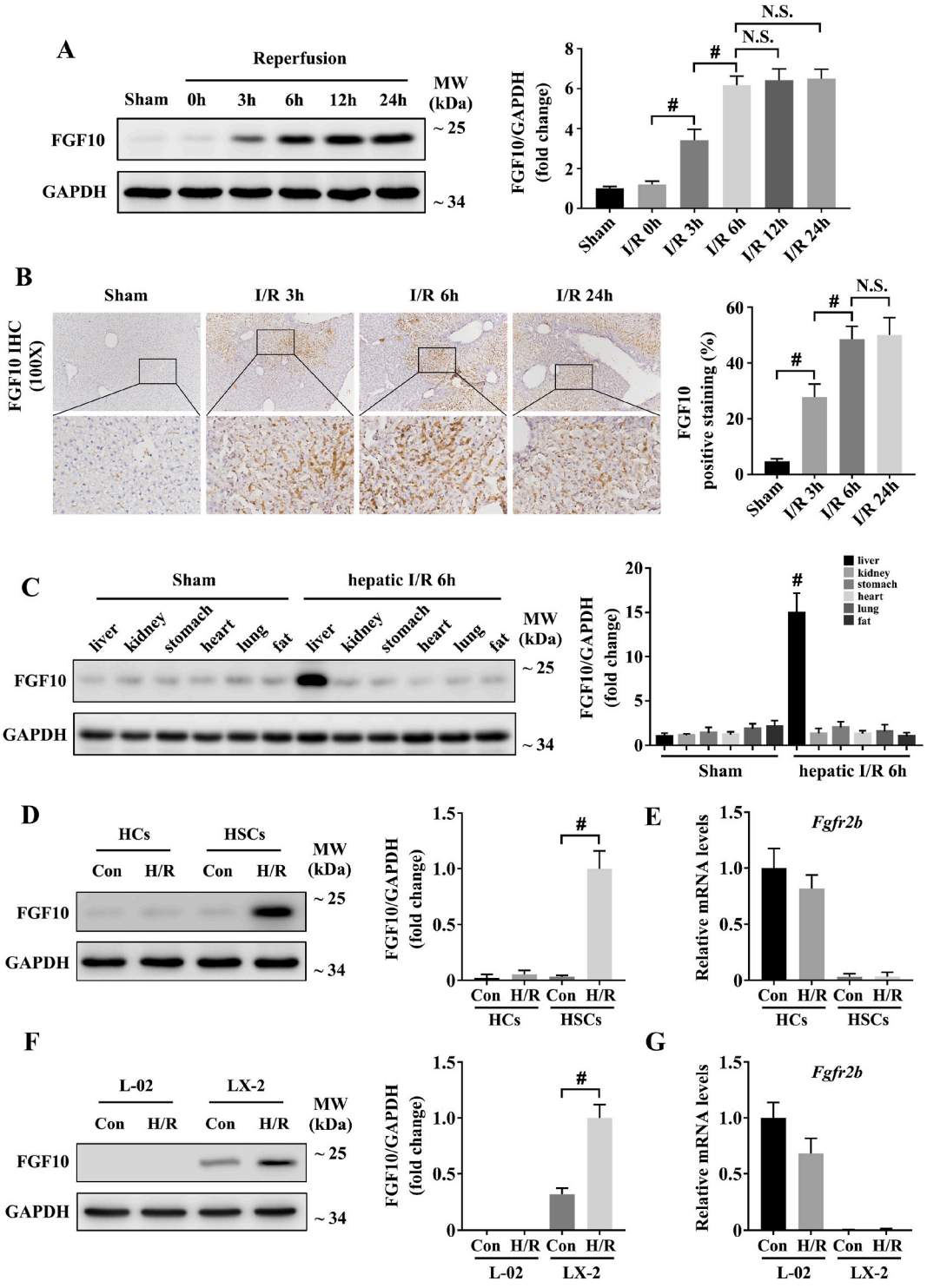

Fig. 1. FGF10 is significantly upregulated during hepatic IRI. (A) Protein expression levels of FGF10 in the livers of mice subjected to sham treatment or ischemia for 90 min followed by indicated periods of reperfusion (n = 4–6 mice/group). (B) Representative IHC staining of FGF10 in the livers of mice after hepatic ischemia for 90 min and reperfusion for 3, 6, and 24 h (n = 4–6 mice/group, magnification × 100). (C) Protein expression levels of FGF10 in major organ samples of mice subjected to sham treatment or 90 min of partial liver warm ischemia followed by 6 h of reperfusion (n = 4–6 mice/group). (D) Protein expression levels of FGF10 in primary hepatocytes and primary HSCs subjected to control or H/R stimulation. (E) The mRNA levels of *Fgfr2b* in primary hepatocytes and primary HSCs subjected to control or H/R stimulation. (F) Protein expression levels of FGF10 in L-02 and LX-2 cells subjected to control or H/R stimulation. (G) The mRNA levels of *Fgfr2b* in L-02 and LX-2 cells subjected to control or H/R stimulation. For (A), (C), (D), and (F), GAPDH was served as the loading control. All data are presented as mean ± SD, $\#P < 0.05$. N.S.: non-significant; Con: control.

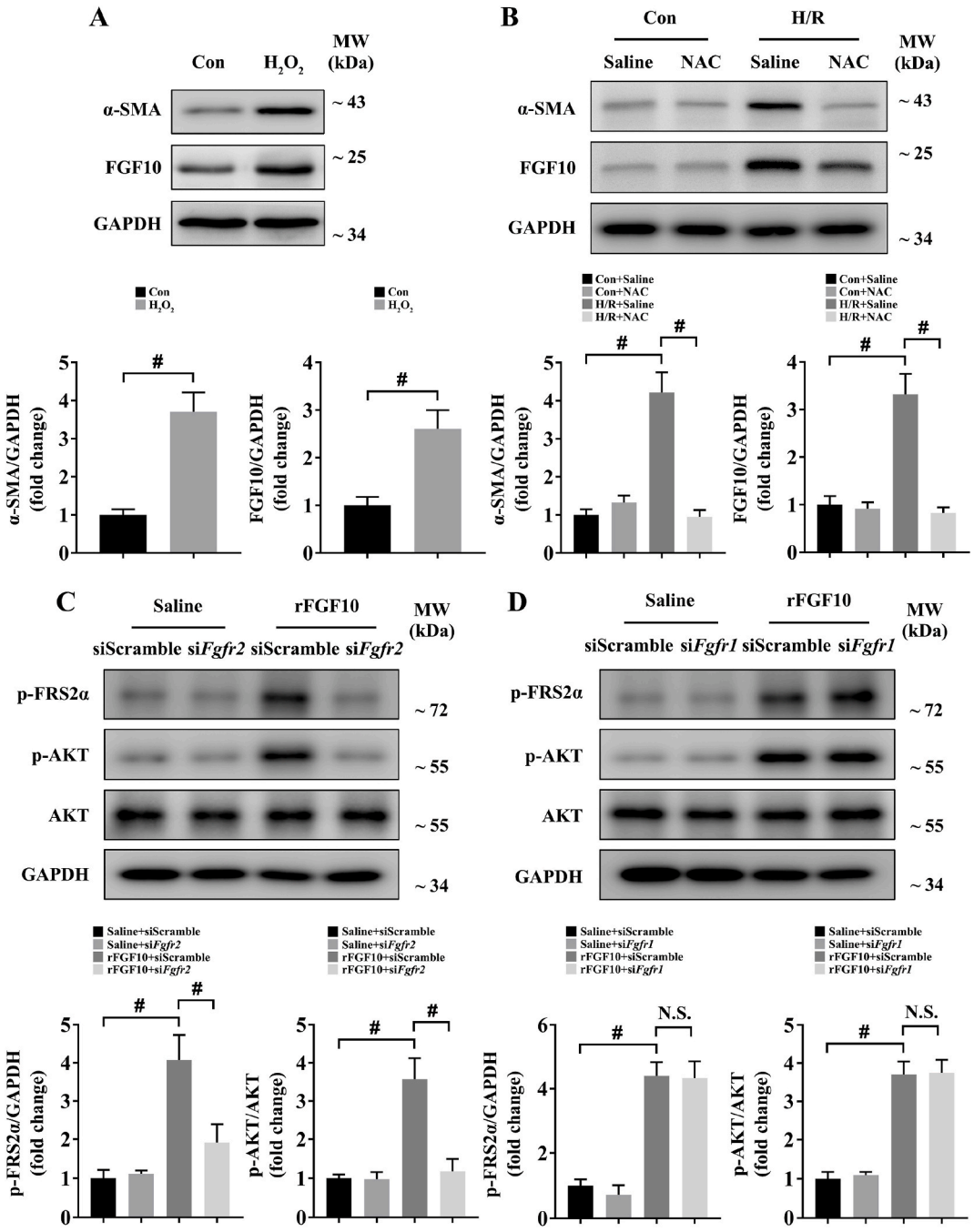

Fig. 2. ROS mediates the expression of FGF10 in HSCs, while FGF10 acts through FGFR2b on hepatocytes. (A) Protein expression levels of α-SMA and FGF10 in primary HSCs treated with or without H_2O_2 (100 μM for 6 h). (B) Protein expression levels of α-SMA and FGF10 in primary HSCs treated with saline or NAC (1 mM added in the culture medium of the reoxygenation phase for 6 h) under control or H/R stimulation. (C) Protein expression levels of phosphorylated FRS2α, phosphorylated AKT, and total AKT in primary hepatocytes transfected with scramble siRNA or FGFR2 siRNA and then treated with saline or rFGF10 (1 μM for 1 h). (D) Protein expression levels of phosphorylated FRS2α, phosphorylated AKT, and total AKT in primary hepatocytes transfected with scramble siRNA or FGFR1 siRNA and then treated with saline or rFGF10 (1 μM for 1 h). For (A–D), GAPDH was served as the loading control; For (C–D), cells were serum starved for 12 h before rFGF10 treatment. All data are presented as mean ± SD, $\#P < 0.05$. Con: control; N.S.: non-significant.

FGF10 overexpression in all kinds of liver cells (Supplementary Fig. 3C), which will possibly lead to FGF10 autocrine signaling in hepatocytes. However, we found that the serum ALT/AST levels and liver architecture were not altered in FGF10-overexpressing mice compared to control mice under normal condition (Supplementary Fig. 4A; Fig. 3A). At 6 h after hepatic IRI, serum levels of ALT and AST were significantly increased in the control group (Supplementary Fig. 4A and B), accompanied by severe liver necrosis as assessed by H&E staining (Fig. 3A). FGF10 overexpression decreased serum ALT and AST levels (Supplementary Fig. 4A), and reduced the necrotic area from approximately 60% to approximately 20% (Fig. 3A). These findings suggest that FGF10 plays a protective role in hepatic IRI. In further support of this conclusion, FGF10 knockdown mice subjected to liver IRI had increased serum levels of ALT and AST (Supplementary Fig. 4B), and increased hepatic necrosis compared with control mice (Fig. 4A).

During hepatic IRI, AKT signaling promotes hepatocyte survival and alleviates liver damage [2,3]. Interestingly, the PI3K/AKT pathway is also the main downstream target of FGF10 signaling [10,12]. Therefore,

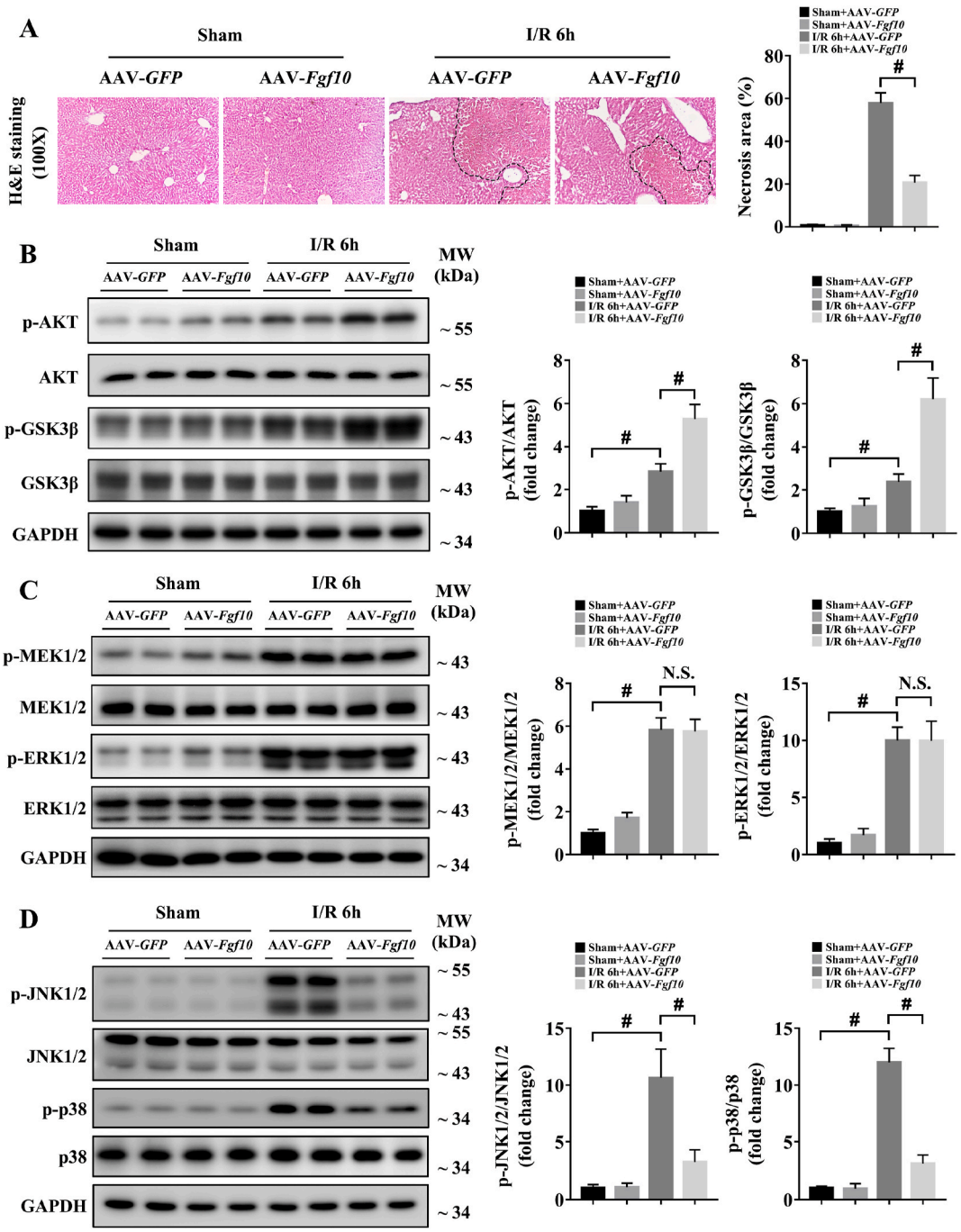

Fig. 3. FGF10 overexpression alleviates liver damage and promotes AKT activation during hepatic IRI. Mice were subjected to 90 min of partial liver warm ischemia, followed by 6 h of reperfusion. (A) Representative H&E staining of liver sections from mice treated with AAV-*GFP*/AAV-*Fgf10* after sham/IRI (magnification × 100). (B) Protein expression levels of AKT signaling in the livers of mice treated with AAV-*GFP*/AAV-*Fgf10* after sham/IRI. (C) Protein expression levels of MEK/ERK signaling in the livers of mice treated with AAV-*GFP*/AAV-*Fgf10* after sham/IRI. (D) Protein expression levels of JNK and p38 signaling in the livers of mice treated with AAV-*GFP*/AAV-*Fgf10* after sham/IRI. For (B–D), GAPDH was served as the loading control. All data are presented as mean ± SD, n = 4–6 mice/group, #$P < 0.05$. N.S.: non-significant.

we tested the role of FGF10 in AKT activation in our model. As shown in Figs. 3B and 4B, FGF10 overexpression significantly increased the phosphorylation of AKT and its downstream target, GSK3β, while FGF10 knockdown decreased AKT and GSK3β phosphorylation. To further confirm whether FGF10 could regulate AKT signaling activation in hepatic IRI, we performed *in vitro* assays in which primary hepatocytes were treated with rFGF10 as well as Transwell experiments with FGF10-knockdown HSCs (Supplementary Fig. 6A and B) in our H/R model. Treatment with rFGF10 activated AKT signaling in primary hepatocytes (Supplementary Fig. 5A and B) after H/R, while knockdown of FGF10 in HSCs impaired AKT activation in primary hepatocytes (Supplementary Fig. 7A and B). Taken together, these results demonstrate that FGF10 plays an essential role in AKT activation during liver IRI.

Furthermore, the MAPK signaling pathway has also been reported to have an important role in the control of hepatic IRI [25,30]. Among the MAPK family members, MAPK/ERK kinase (MEK) and extracellular-signal-regulated kinase (ERK) are known downstream

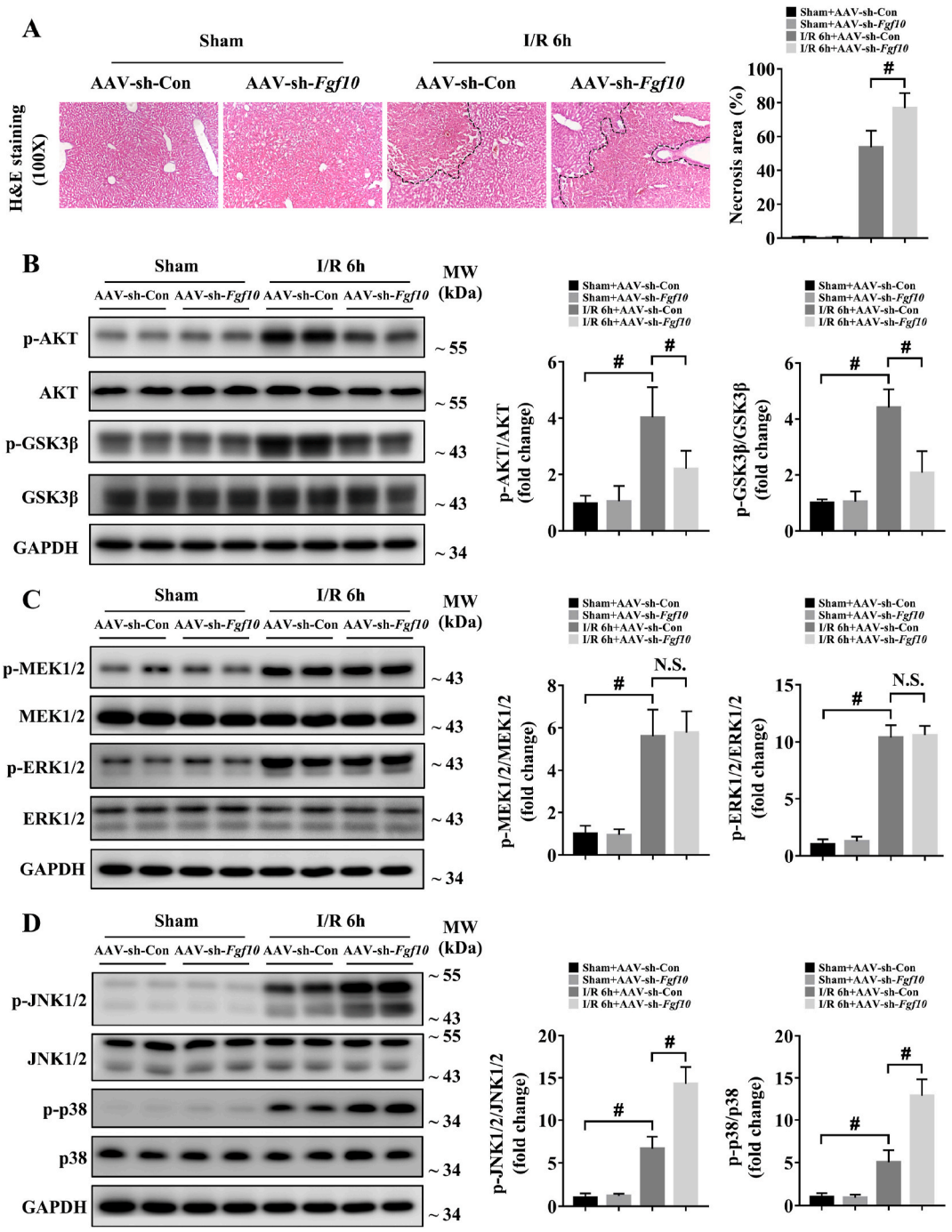

Fig. 4. FGF10 knockdown aggravates liver damage and impairs AKT activation during hepatic IRI. Mice were subjected to 90 min of partial liver warm ischemia, followed by 6 h of reperfusion. (A) Representative H&E staining of liver sections from mice treated with AAV-sh-Con/AAV-sh-*Fgf10* after sham/IRI (magnification × 100). (B) Protein expression levels of AKT signaling in the livers of mice treated with AAV-sh-Con/AAV-sh-*Fgf10* after sham/IRI. (C) Protein expression levels of MEK/ERK signaling in the livers of mice treated with AAV-sh-Con/AAV-sh-*Fgf10* after sham/IRI. (D) Protein expression levels of JNK and p38 signaling in the livers of mice treated with AAV-sh-Con/AAV-sh-*Fgf10* after sham/IRI. For (B–D), GAPDH was served as the loading control. All data are presented as mean ± SD, n = 4–6 mice/group, $\#P < 0.05$. N.S.: non-significant.

targets of FGF10 [10,12]. Thus, we evaluated the status of four MAPK family members (MEK, ERK, JNK and p38) in our mouse model of hepatic IRI. As shown in Fig. 3C and D and Fig. 4C and D, western blot analysis demonstrated that the phosphorylation of MEK1/2, ERK1/2, JNK1/2 and p38 were increased at 6 h after hepatic IRI, indicating the injured state of the liver. Surprisingly, FGF10 overexpression and knockdown had no effect on MEK/ERK activation during liver IRI (Figs. 3C and 4C). However, FGF10 overexpression significantly ameliorated the activation of JNK1/2 and p38 (Fig. 3D), while FGF10 knockdown increased the phosphorylation of JNK1/2 and p38 after hepatic IRI (Fig. 4D). Accompany with the *in vivo* results, treatment with rFGF10 (Supplementary Fig. 5A and B) or silencing of FGF10 (Supplementary Fig. 7A and B) also had no effect on the activation of MEK/ERK in primary hepatocytes after H/R, but affected the JNK1/2 and p38 pathways.

3.4. FGF10 protects hepatocytes from apoptosis during the injury phase and promotes hepatocyte proliferation during the recovery phase of liver IRI

Cellular apoptosis directly contributes to liver damage during hepatic IRI [18,25,30]. Recent studies demonstrated that FGF10 can inhibit neuronal apoptosis during cerebral IRI [31], suggesting a possible role for FGF10 in the regulation of apoptosis after liver IRI. In our study, TUNEL staining revealed that the number of apoptotic cells significantly increased in control mice at 6 h after hepatic IRI, while FGF10 overexpression significantly reduced hepatocyte apoptosis (Fig. 5A). Moreover, the level of c-CAS-3 and the ratio between the pro-apoptotic protein Bax and the anti-apoptotic protein Bcl-2 were also dramatically decreased in the FGF10-overexpressing mice after liver IRI (Fig. 5B). By contrast, FGF10 knockdown increased apoptosis at 6 h after hepatic IRI compared with the control group, as evidenced by an increase in TUNEL-positive nuclei, a higher Bax/Bcl-2 ratio, and higher levels of c-CAS-3 (Fig. 6A and B). In parallel, these results were

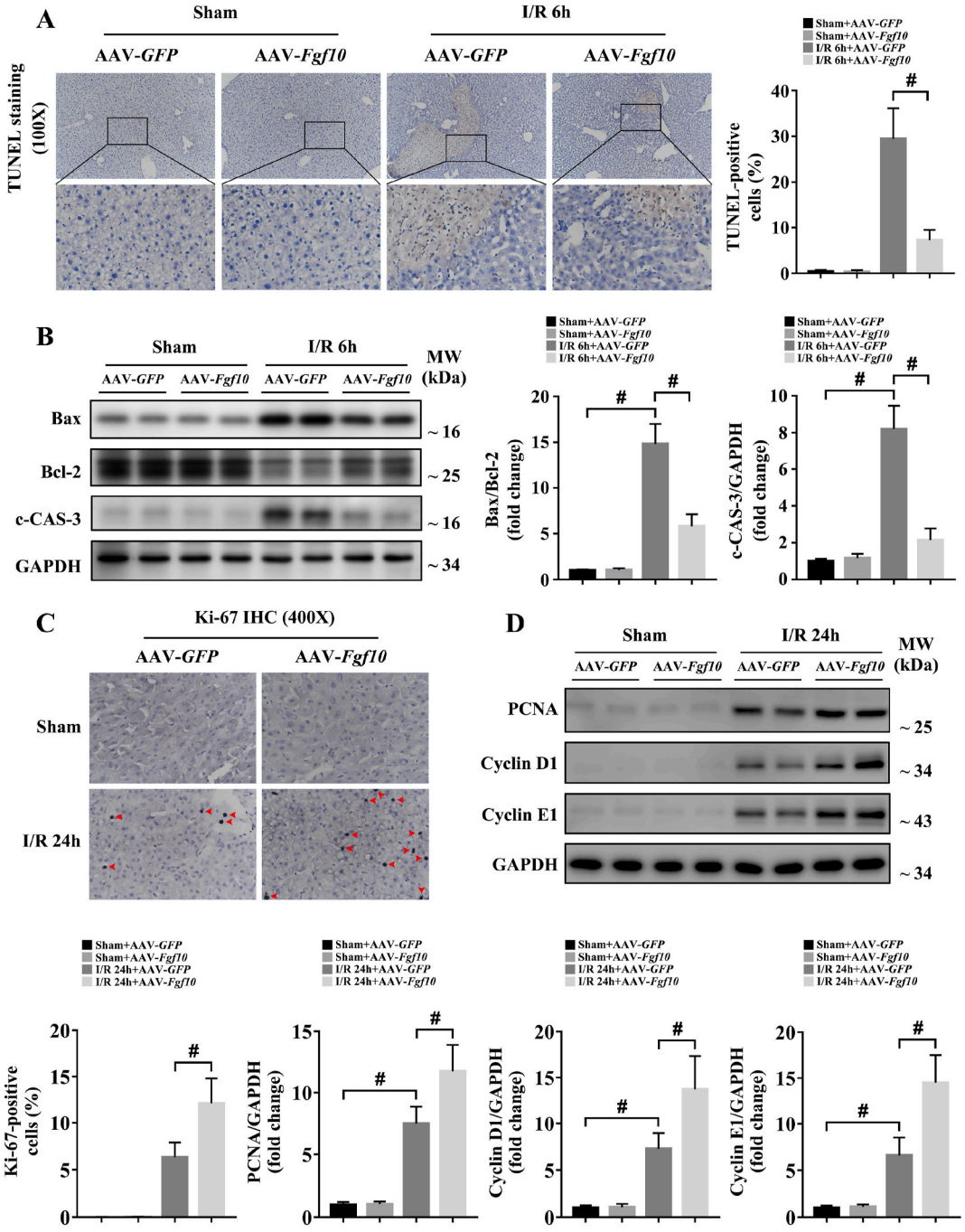

Fig. 5. FGF10 overexpression protects hepatocytes from apoptosis during the injury phase and promotes hepatocyte proliferation during the recovery phase of liver IRI. Mice were subjected to 90 min of partial liver warm ischemia, followed by 6 h or 24 h of reperfusion. (A) Representative TUNEL staining of liver sections from mice treated with AAV-*GFP*/AAV-*Fgf10* after sham/IRI (magnification × 100). (B) Protein expression levels of Bax, Bcl-2, and c-CAS-3 in the livers of mice treated with AAV-*GFP*/AAV-*Fgf10* after sham/IRI. (C) Representative Ki-67 IHC staining of liver sections from mice treated with AAV-*GFP*/AAV-*Fgf10* after sham/IRI (magnification × 400). (D) Protein expression levels of PCNA, cyclin D1, and cyclin E1 in the livers of mice treated with AAV-*GFP*/AAV-*Fgf10* after sham/IRI. For (B) and (D), GAPDH was served as the loading control. All data are presented as mean ± SD, n = 4–6 mice/group, $\#P < 0.05$.

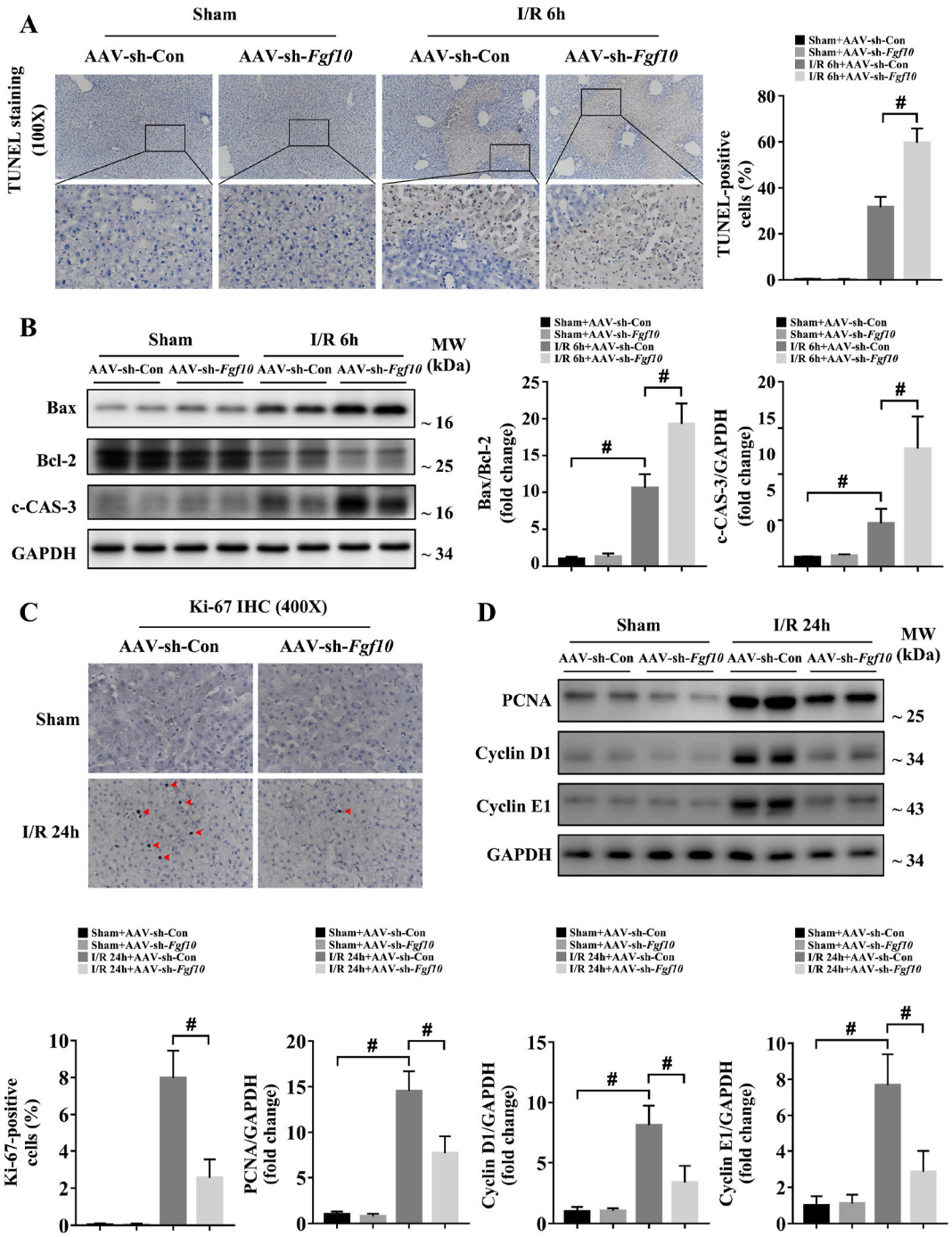

Fig. 6. FGF10 knockdown aggravates hepatocellular apoptosis during the injury phase and impairs hepatocyte proliferation during the recovery phase of liver IRI. Mice were subjected to 90 min of partial liver warm ischemia, followed by 6 h or 24 h of reperfusion. (A) Representative TUNEL staining of liver sections from mice treated with AAV-sh-Con/AAV-sh-*Fgf10* after sham/IRI (magnification × 100). (B) Protein expression levels of Bax, Bcl-2, and c-CAS-3 in the livers of mice treated with AAV-sh-Con/AAV-sh-*Fgf10* after sham/IRI. (C) Representative Ki-67 IHC staining of liver sections from mice treated with AAV-sh-Con/AAV-sh-*Fgf10* after sham/IRI (magnification × 400). (D) Protein expression levels of PCNA, cyclin D1, and cyclin E1 in the livers of mice treated with AAV-sh-Con/AAV-sh-*Fgf10* after sham/IRI. For (B) and (D), GAPDH was served as the loading control. All data are presented as mean ± SD, n = 4–6 mice/group, #$P < 0.05$.

confirmed in primary hepatocytes. As shown in Supplementary Fig. 5A and B and Supplementary Fig. 7A and B, rFGF10 treatment down-regulated the Bax/Bcl-2 ratio and the level of c-CAS-3 after H/R, while FGF10 silencing increased the level of c-CAS-3 and the Bax/Bcl-2 ratio after H/R. Taken together, these results suggest that FGF10 inhibits hepatocellular apoptosis during liver IRI.

Hepatocyte proliferation/regeneration is a key process in liver recovery after IRI [4,5], and FGF10 also has the ability to control liver development and regeneration [13,14]. Therefore, we determined the effect of FGF10 on hepatocyte proliferation during liver IRI. As hepatocytes mostly proliferate during the recovery phase of IRI, this experiment was performed 24 h after liver IRI. Ki-67 staining revealed that FGF10 overexpression did not promote hepatocyte proliferation under normal condition, but increased the proliferation of hepatocytes after IRI (Fig. 5C). This result was further confirmed by western blot analysis of proliferating cell nuclear antigen (PCNA), cyclin D1, and cyclin E1 (Fig. 5D). Meanwhile, FGF10 loss of function inhibited liver regeneration after IRI, as evidenced by a decrease in Ki-67-positive nuclei after

hepatic IRI (Fig. 6C), and decreased protein expression of PCNA, cyclin D1, and cyclin E1 (Fig. 6D). These experiments suggest that FGF10 is a pivotal factor controlling hepatocyte proliferation after liver IRI.

3.5. FGF10 reduces inflammatory responses during hepatic IRI

During hepatic IRI, inflammation occurs in response to tissue injury and influences liver function and recovery [3,4,18,30]. We first used IHC to evaluate the degree of inflammation in the liver at 6 h after IRI in our mouse models. Expression of the macrophage marker CD68 and the neutrophil marker MPO were both markedly increased during hepatic IRI in the control group (Fig. 7A and Fig. 8A), indicating an obvious inflammatory response in the liver, while FGF10 overexpression resulted in decreased macrophage and neutrophil infiltration after IRI (Fig. 7A). As NF-κB signaling activation contributes to hepatic injury and is closely related with the generation of inflammatory factors, we thus used western blotting to analyze the phosphorylation of IκBα and p65, and found that FGF10 overexpression significantly reduced NF-κB activation at 6 h after IRI (Fig. 7B). In addition, the production of inflammatory cytokines (*Tnf-α*, *Il-1β* and *Il-6*) and chemokines (*Ccl2* and *Cxcl2*) in response to hepatic IRI was also decreased by FGF10 overexpression (Fig. 7C). By contrast, FGF10 knockdown increased infiltration of the

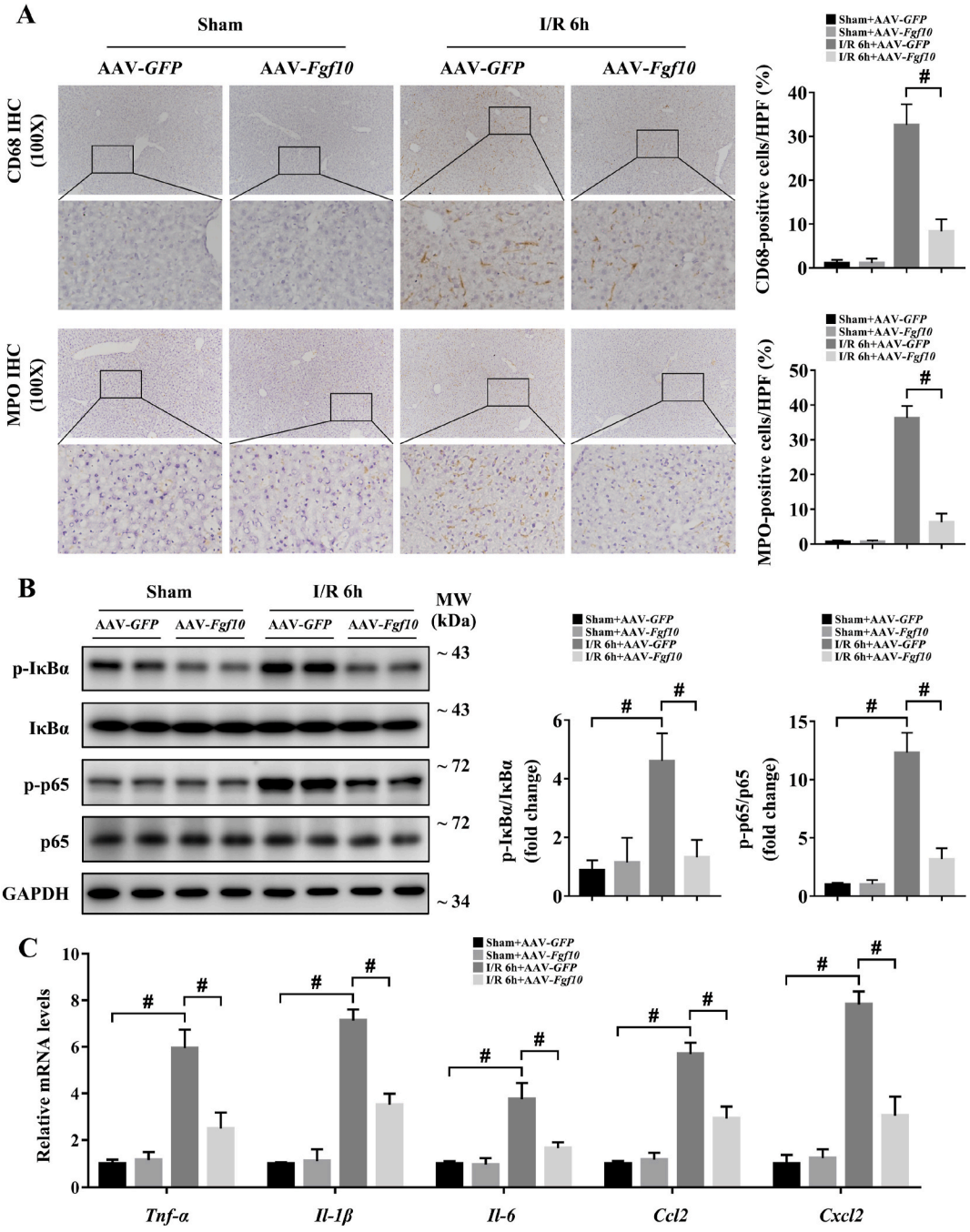

Fig. 7. FGF10 overexpression reduces inflammatory responses during hepatic IRI. Mice were subjected to 90 min of partial liver warm ischemia, followed by 6 h of reperfusion. (A) Representative CD68 and MPO IHC staining of liver sections from mice treated with AAV-*GFP*/AAV-*Fgf10* after sham/IRI (magnification × 100). (B) Protein expression levels of NF-κB signaling in the livers of mice treated with AAV-*GFP*/AAV-*Fgf10* after sham/IRI (GAPDH was served as the loading control). (C) The mRNA levels of pro-inflammatory factors (*Tnf-α*, *Il-1β*, *Il-6*, *Ccl2*, and *Cxcl2*) in the livers of mice treated with AAV-*GFP*/AAV-*Fgf10* after sham/IRI. All data are presented as mean ± SD, n = 4–6 mice/group, $\#P < 0.05$.

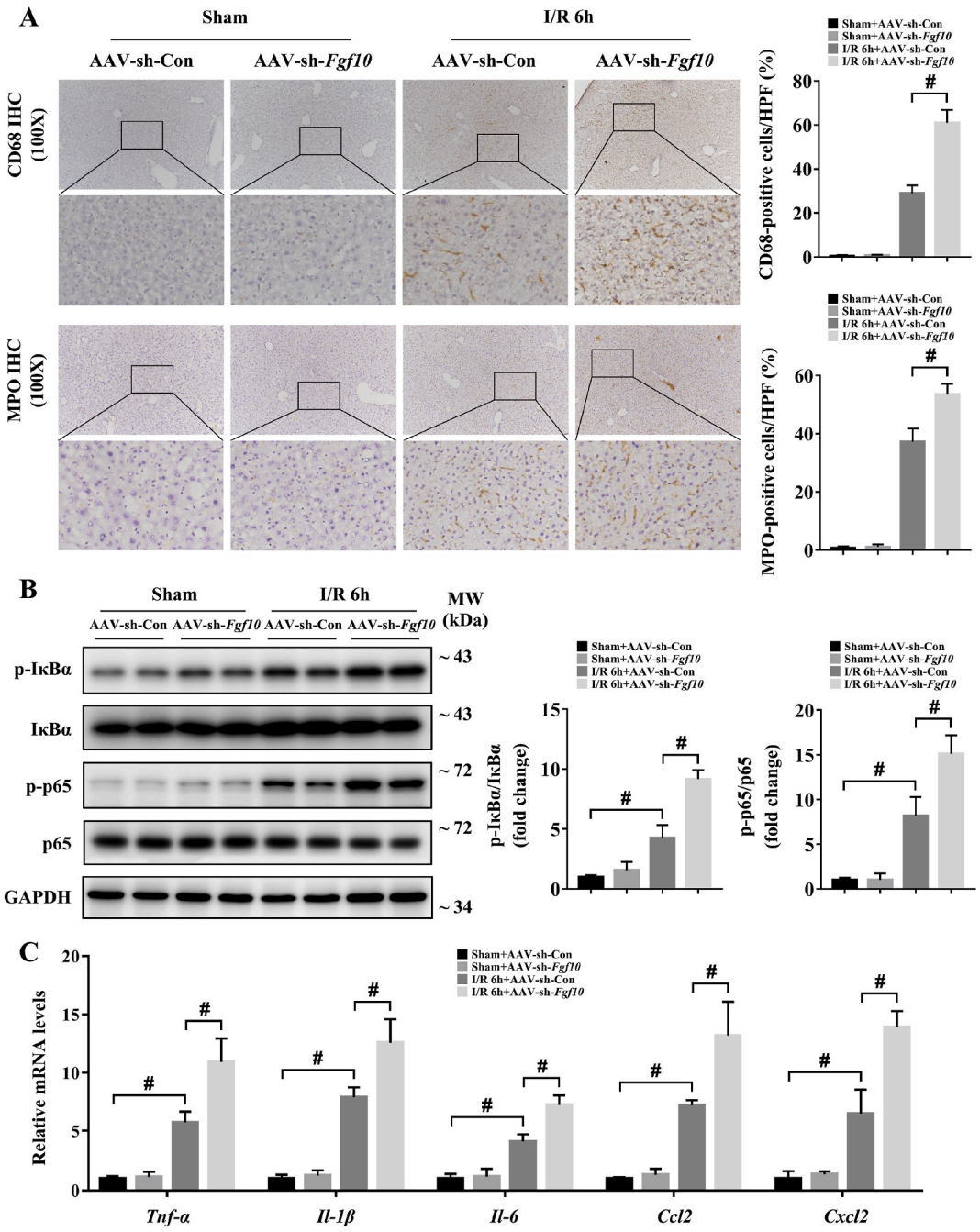

Fig. 8. FGF10 knockdown aggravates inflammatory responses during hepatic IRI. Mice were subjected to 90 min of partial liver warm ischemia, followed by 6 h of reperfusion. (A) Representative CD68 and MPO IHC staining of liver sections from mice treated with AAV-sh-Con/AAV-sh-*Fgf10* after sham/IRI (magnification × 100). (B) Protein expression levels of NF-κB signaling in the livers of mice treated with AAV-sh-Con/AAV-sh-*Fgf10* after sham/IRI (GAPDH was served as the loading control). (C) The mRNA levels of pro-inflammatory factors (*Tnf-α*, *Il-1β*, *Il-6*, *Ccl2*, and *Cxcl2*) in the livers of mice treated with AAV-sh-Con/AAV-sh-*Fgf10* after sham/IRI. All data are presented as mean ± SD, n = 4–6 mice/group, #$P < 0.05$.

liver by macrophages and neutrophils, enhanced NF-κB signaling, and increased the expression of *Tnf-α*, *Il-1β*, *Il-6*, *Ccl2,* and *Cxcl2* (Fig. 8A–C). Consistent with these *in vivo* studies, treatment of hepatocytes with rFGF10 decreased the phosphorylation of IκBα and p65 after H/R (Supplementary Fig. 5A and B), and FGF10 silencing increased NF-κB activation (Supplementary Fig. 7A and B). These data suggest that FGF10 plays an anti-inflammatory role during hepatic IRI.

3.6. FGF10 inhibits oxidative stress and activates NRF2 via AKT signaling during hepatic IRI

During hepatic IRI, ROS accumulate early in the reperfusion stage [4,6,18]. ROS promote several cellular processes that exacerbate liver damage, including apoptosis, inflammation, and metabolism disequilibrium [4,6,17,19]. Interestingly, we found that FGF10 was highly expressed during the early phase of hepatic IRI and ROS led to FGF10 production in HSCs. Thus, we assessed whether FGF10 expression could affect oxidative stress in liver IRI. DHE staining showed that ROS production was highly inhibited by FGF10 overexpression at 6 h after IRI

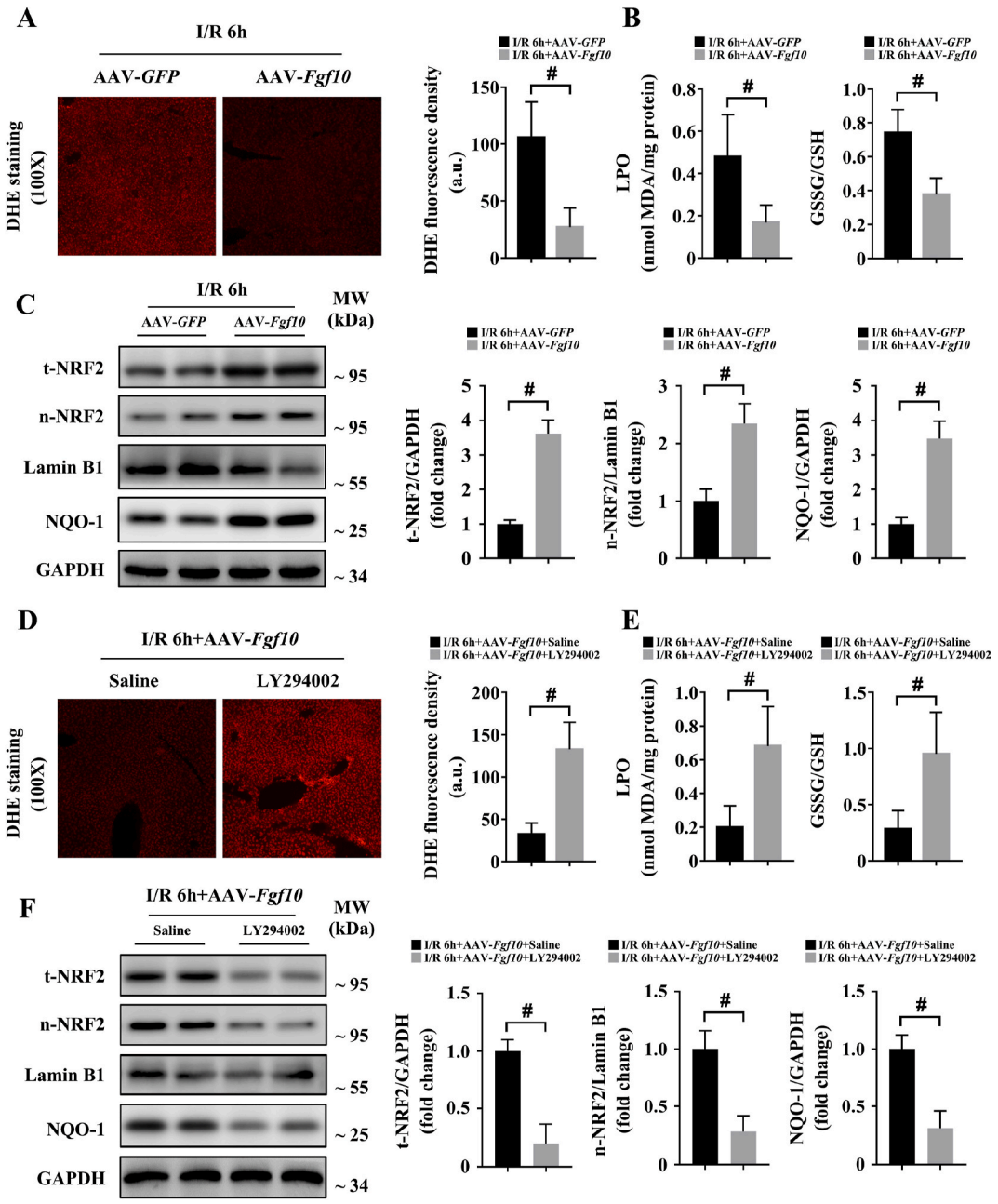

Fig. 9. FGF10 inhibits oxidative stress and activates NRF2 via AKT signaling during hepatic IRI. Mice were subjected to 90 min of partial liver warm ischemia, followed by 6 h of reperfusion. (A) Representative DHE staining of liver sections from mice treated with AAV-*GFP*/AAV-*Fgf10* after IRI (magnification × 100). (B) Levels of LPO and GSSG/GSH ratio in the livers of mice treated with AAV-*GFP*/AAV-*Fgf10* after IRI. (C) Protein expression levels of total NRF2, nuclear NRF2, and NQO-1 in the livers of mice treated with AAV-*GFP*/AAV-*Fgf10* after IRI. (D) Representative DHE staining of liver sections from AAV-*Fgf10* transfected mice treated with saline or LY294002 after IRI (magnification × 100). (E) Levels of LPO and GSSG/GSH ratio in the livers of AAV-*Fgf10* transfected mice treated with saline or LY294002 after IRI. (F) Protein expression levels of total NRF2, nuclear NRF2, and NQO-1 in the livers of AAV-*Fgf10* transfected mice treated with saline or LY294002 after IRI. For (C) and (F), GAPDH and Lamin B1 were served as the loading control, respectively. All data are presented as mean ± SD, n = 4–6 mice/group, $\#P < 0.05$. t-NRF2: total NRF2; n-NRF2: nuclear NRF2.

(Fig. 9A). Meanwhile, levels of LPO and oxidized/total glutathione ratio, which are intracellular markers of redox status, were both decreased in FGF10-overexpressing animals (Fig. 9B), indicating that FGF10 had an inhibitory effect on ROS production during hepatic IRI. Given that FGF10 is not a direct antioxidant, and considering the previously reported strong anti-oxidative role of NRF2 in IRI, we used western blotting to assess the relationship between FGF10 and NRF2. As shown in Fig. 9C, the protein levels of total NRF2 and nuclear NRF2 were both upregulated in FGF10-overexpressing mouse liver tissues after IRI, as well as NQO-1, the downstream target of NRF2. Additionally, in primary hepatocytes, DCFH-DA staining and western blotting demonstrated that FGF10 markedly decreased ROS production and upregulated both total NRF2 and nuclear NRF2 protein expression after H/R stimulation (Supplementary Fig. 8A and B). Together, these results indicate that FGF10 overexpression can lead to NRF2 activation during liver IRI.

Given that AKT is an important upstream regulator of NRF2 [22], and FGF10 highly induced the phosphorylation of AKT, we hypothesized that FGF10 activated NRF2 through PI3K/AKT signaling. To obtain this, we found that pre-treatment with PI3K inhibitor LY294002 abolished the anti-oxidative effects of FGF10 in liver IRI, as demonstrated by DHE

staining, together with measurement of the LPO level and the oxidized/total glutathione ratio (Fig. 9D and E). In addition, administration of LY294002 markedly decreased the protein expression of total NRF2, nuclear NRF2, and NQO-1 in FGF10-overexpressing mice after hepatic IRI (Fig. 9F). For *in vitro* experiments, rFGF10 treatment had no effect on ROS levels or NRF2 activation after H/R in the presence of LY294002 (Supplementary Fig. 8C and D). Furthermore, LY294002 abrogated the protective effects of FGF10 overexpression in mice, as determined by serum ALT/AST levels and the measurement of liver necrosis at 6 h after IRI (Supplementary Fig. 9A and B). Taken together, these results indicate that FGF10 overexpression activates NRF2 through the PI3K/AKT signaling and thus protecting the liver during IRI.

3.7. NRF2 is required for FGF10-mediated hepatocellular protection in liver IRI

Considering that FGF10 induced NRF2 activation in hepatic IRI, and that NRF2 is a master regulator of liver injury during IRI [17,19], we asked whether the protective effects of FGF10 in IRI were dependent on NRF2. Thus, NRF2 knockout mice with or without FGF10 overexpression were subjected to warm IRI. FGF10 failed to protect the liver at 6 h post-IRI in NRF2 knockout mice, as FGF10-overexpressing mice

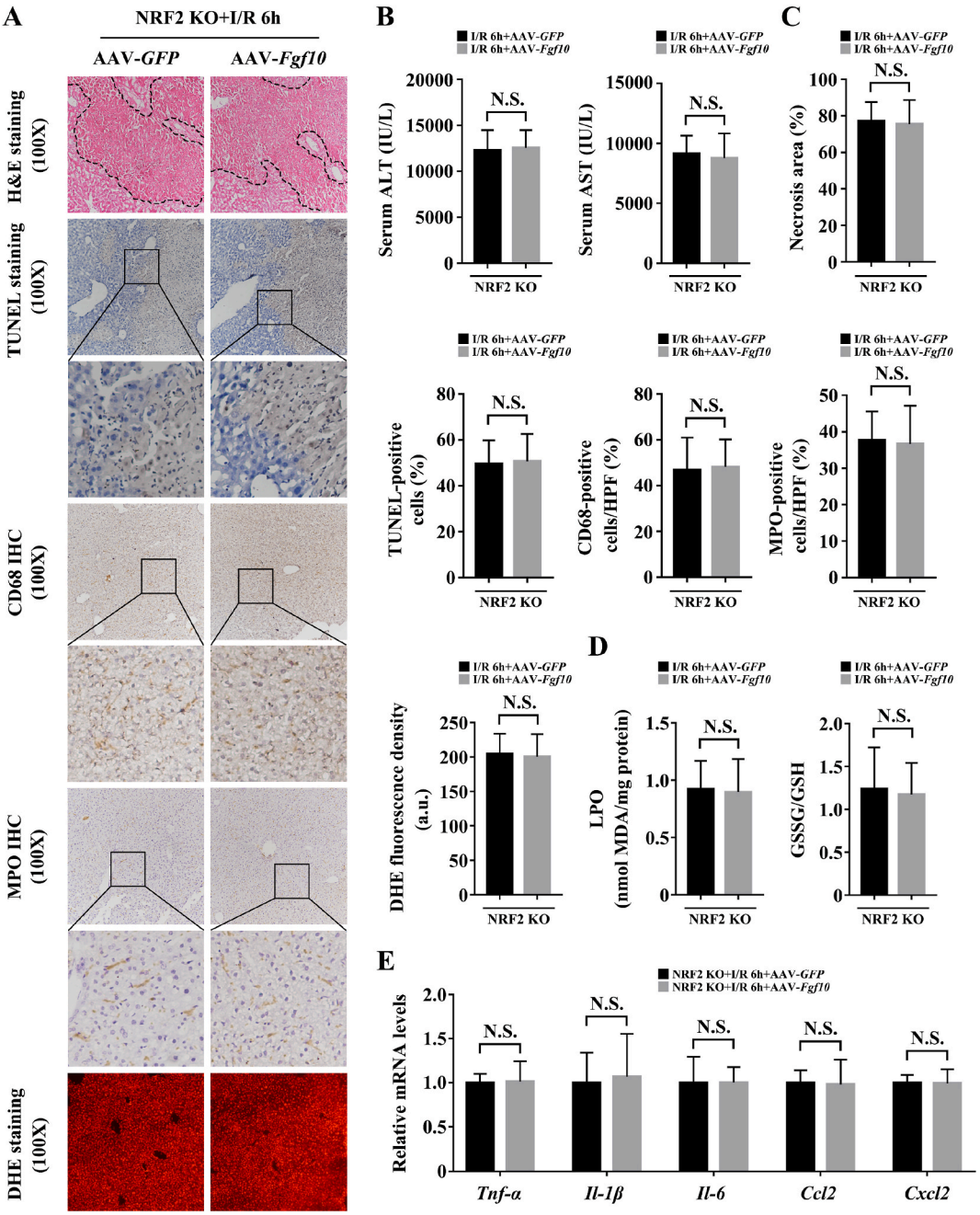

Fig. 10. NRF2 is required for FGF10-mediated hepatocellular protection in liver IRI. Mice were subjected to 90 min of partial liver warm ischemia, followed by 6 h of reperfusion. (A) Representative H&E staining, TUNEL staining, CD68 IHC staining, MPO IHC staining, and DHE staining of liver sections from NRF2 knockout mice treated with AAV-*GFP*/AAV-*Fgf10* after IRI (magnification × 100). (B) Serum levels of ALT and AST in NRF2 knockout mice treated with AAV-*GFP*/AAV-*Fgf10* after IRI. (C) Statistical results of panel A. (D) Levels of LPO and GSSG/GSH ratio in the livers of NRF2 knockout mice treated with AAV-*GFP*/AAV-*Fgf10* after IRI. (E) The mRNA levels of pro-inflammatory factors (*Tnf-α*, *Il-1β*, *Il-6*, *Ccl2*, and *Cxcl2*) in the livers of NRF2 knockout mice treated with AAV-*GFP*/AAV-*Fgf10* after IRI. All data are presented as mean ± SD, n = 4–6 mice/group. N.S.: non-significant.

had similar levels of necrosis, serum ALT/AST, cellular apoptosis, macrophage/neutrophil infiltration, and ROS as the control group (Fig. 10A–D). Moreover, the production of pro-inflammatory cytokines and chemokines after hepatic IRI were also similar in NRF2 knockout mice treated with AAV-*GFP* or AAV-*Fgf10* (Fig. 10E). Western blotting revealed that in NRF2 knockout mice, overexpression of FGF10 activated PI3K/AKT at 6 h post-IRI but had no effect on the activation of JNK, p38, IκBα, or p65, and also did not affect the Bax/Bcl-2 ratio or the level of c-CAS-3 (Supplementary Fig. 10A and B). Furthermore, the pro-proliferative effects of FGF10 in the late phase of liver IRI were also abrogated in NRF2 knockout mice, as measured by Ki-67 staining and the protein expression of PCNA, cyclin D1, and cyclin E1 at 24 h post-IRI (Supplementary Fig. 11A and B). These results demonstrate that NRF2 activation is critical for the protective effects of FGF10 in hepatic IRI.

4. Discussion

FGF10 has been shown to protect against ischemic injury in the brain, lung, and kidney [31–33]. FGF10 is also critical for organ development during embryogenesis, and contributes to tissue repair and wound healing in adult mice [10,12,13]. In the present study, we showed that overexpression of FGF10 in mice significantly preserved liver function after IRI, as evidenced by diminished serum ALT/AST levels, reduced necrosis, increased hepatocyte proliferation, decreased cellular apoptosis, reduced inflammation, and decreased oxidative stress. By contrast, knockdown of FGF10 aggravated liver injury after IRI. Our results provide the first evidence that FGF10 is an important mediator of hepatic IRI and plays a pivotal role in ameliorating liver injury after ischemia-reperfusion, and we also reveal that the protective effects of FGF10 against liver IRI are closely related with NRF2 activation.

FGF10 is expressed in the mesenchymal tissue of the liver [13], while its receptor, FGFR2b, is expressed in the epithelial tissue [12,13,26]. Consistent with this, our results indicated that HSCs were the source of FGF10 during IRI, since FGF10 was mostly expressed in HSCs after H/R stimulation. Meanwhile, we also showed that ROS mediated HSC activation and the subsequent FGF10 expression. In a recent study of a warm liver IRI model, HSCs in the periportal areas started to proliferate at 24 h after reperfusion, and the proliferation rate peaked at 48 h after reperfusion [34]. Our IHC staining and western blotting results indicated that FGF10 was mostly produced in the necrotic areas of the liver, and its expression peaked at 6 h after IRI, indicating that HSCs in the necrotic tissue produce FGF10 at an early phase after reperfusion in hepatic IRI.

Both PI3K/AKT and MEK/ERK signaling play important roles in the pathological process of liver IRI [2,3,35,36]. AKT activation has been shown to be required for the protective effects of some therapeutic approaches targeting liver IRI, such as ischemic preconditioning and helium preconditioning [2,3], while MEK/ERK signaling is thought to promote apoptosis and inflammation in liver IRI [35,36]. Interestingly, FGF10 can induce both PI3K/AKT and MEK/ERK activation in many organs [10,12], making it difficult to judge its effects in hepatic IRI. In our study, FGF10 overexpression strongly induced AKT signaling during liver IRI but had no obvious effects on MEK/ERK activation, and the expression of FGF10 during liver IRI was also critical for AKT activation, as knockdown of FGF10 impaired AKT signaling activation after IRI. Furthermore, pharmacological inhibition of AKT activation abolished the protective effects of FGF10 overexpression, indicating the necessary role of AKT in FGF10-mediated protection during hepatic IRI.

Hepatocyte apoptosis and proliferation are considered important hallmarks during liver IRI [4,5,18,25,30]. In the early stages of reperfusion, inflammatory responses and ROS production directly leads to hepatocellular apoptosis [4,6], while in the late stages of reperfusion, hepatocyte proliferation contributes to liver repair and critically maintains liver function [4,5]. An imbalance between apoptosis and proliferation will aggravate hepatic injury in IRI [37]. FGF10 has been shown to prevent apoptosis and promote proliferation in many diseases [10], in our study, similarly, FGF10 showed powerful anti-apoptotic effects in the early acute injury phase of liver IRI, and it also exerted strong pro-proliferative effects in the recovery phase of hepatic IRI, these properties of FGF10 make it represent well potential in the clinical treatment of hepatic IRI.

Hepatic IRI is also characterized by sterile inflammation [3], in which macrophages and neutrophils recruited to the post-ischemic liver damage hepatocytes by producing oxidants and proteases. The expression of anti-inflammatory mediators has been shown to play a critical role in the resolution of injury [4]. Our study indicated FGF10 prevented immune cell infiltration, inhibited NF-κB activation, and decreased the production of inflammatory cytokines and chemokines in hepatic IRI, while FGF10 knockdown had the opposite effects. However, it is hard to say that FGF10 inhibits NF-κB signaling and thus reducing inflammation, as the reduced levels of cytokines (of which may activate NF-κB, such as TNF-α) are also responsible for the reduced NF-kB activation [38]. Nevertheless, our results suggest that FGF10 exerts great anti-inflammatory properties during hepatic IRI and it may be considered as an innate anti-inflammatory mediator in the liver.

During liver IRI, anoxia followed by reoxygenation directly affects metabolism and results in massive ROS production. ROS can induce protein oxidation and DNA damage, and they can also act as signaling molecules, activating several downstream targets, including JNK, p38, and NF-κB [4,6,7,39], and thus inducing apoptosis and inflammation. Studies have indicated that the generation of ROS scavengers such as catalase and MnSOD is beneficial in hepatic IRI [6,19]. In our study, FGF10 markedly reduced oxidative stress by activating NRF2 signaling via the PI3K/AKT pathway in hepatic IRI, and thus preventing ROS induced hepatocellular apoptosis and inflammation. The relationship between NRF2 activation and AKT signaling pathway is complicated, for example, AKT signaling activation can inhibit the export and degradation of nuclear NRF2 through the GSK-3β/Fyn pathway [40], and it can also induce NRF2 phosphorylation, resulting in stabilization of the protein [41]. Our results showed that the protein levels of total NRF2 and nuclear NRF2 were both upregulated upon FGF10 overexpression/treatment, indicating that FGF10 contributes to oxidant-antioxidant homeostasis in the liver through mediating NRF2 activation.

It was previously reported that NRF2 can alleviate hepatocellular damage in IRI, and NRF2 knockout liver grafts were more susceptible to ischemia-reperfusion [17,19]. NRF2 can not only regulate antioxidant defenses, but also affect autophagy, metabolism, and mitochondrial bioenergetics [42,43]. In NRF2 knockout mice, FGF10 overexpression failed to protect against liver IRI from necrosis, hepatic dysfunction, hepatocellular apoptosis, and inflammatory response. Furthermore, our results also demonstrated that the pro-proliferative effects of FGF10 in the recovery phase of liver IRI were abrogated by NRF2 knockout, consistent with the previous notion that NRF2 could regulate liver regeneration after partial hepatectomy through reduction of ROS levels [44]. It is hard to say that the protective effects of FGF10 against hepatic IRI is totally dependent on NRF2 activation, as in our experiment, the damage in the NRF2 knockout mice may simply be too high to allow an effect of FGF10, and the other downstream targets of AKT signaling, like β-catenin, has also been proved to have a protective effect against liver IRI [45]. Nevertheless, our results indicate that NRF2 activation is a prerequisite for the protective effects of FGF10 during hepatic IRI, including its effects on hepatocyte proliferation.

It should be noted that the AAV-mediated gene overexpression and knockdown in our study were a systemic effect. Although we showed that the liver is the main site of FGF10 secretion during hepatic IRI, it is still possible that extrahepatic events may contribute to this model. In addition, we found that the AAV-mediated FGF10 overexpression was achieved in all kinds of liver cells in our mouse models (possibly because of the non-specific CMV promoter), which might induce autocrine FGF10 signaling in hepatocytes. Fortunately, no significant difference was obtained by FGF10 overexpression in normal mouse livers. Also, as

the production of FGF10 is mostly mediated by HSCs, it is difficult to use AAV to achieve cell-specific gene transfer. Although some studies have used several specific promoters, including glial fibrillary acidic protein, to specifically target HSCs [46], this method may also target other types of cells, including ductular cells and cholangiocytes [47].

In summary, our study demonstrates the protective effects of FGF10 in liver IRI. FGF10 induction and the subsequent AKT-dependent NRF2 activation contribute to liver repair and may be essential for the maintenance of hepatic homeostasis after IRI, and FGF10 inhibition may also have an adverse effect in the treatment of IRI. These findings could broaden our understanding of the regulatory role of FGF10 in the liver and support FGF10 as a novel molecular target for future therapeutic approaches against hepatic IRI.

Funding

This work was supported by the National Natural Science Foundation of China (82070507, 81673077, 81773346, and 81770498), the Key Scientific Project of MOST, China (2017YFA0506000), the Zhejiang Provincial Natural Science Foundation of China (LZ21H020002, LQ21H020010), the Zhejiang Province Medical and Health Science Program (2018KY504), and the Science and Technology Bureau Project of Wenzhou (Y20190175).

Declaration of competing interest

The authors declare that they have no known competing financial interests or personal relationships that could have appeared to influence the work reported in this paper.

Appendix A. Supplementary data

Supplementary data to this article can be found online at https://doi.org/10.1016/j.redox.2021.101859.

References

[1] S. Kuboki, T. Shin, N. Huber, et al., Peroxisome proliferator-activated receptor-gamma protects against hepatic ischemia/reperfusion injury in mice, Hepatology 47 (2008) 215–224.
[2] K. Izuishi, A. Tsung, M.A. Hossain, et al., Ischemic preconditioning of the murine liver protects through the Akt kinase pathway, Hepatology 44 (2006) 573–580.
[3] R. Zhang, L. Zhang, A. Manaenko, et al., Helium preconditioning protects mouse liver against ischemia and reperfusion injury through the PI3K/Akt pathway, J. Hepatol. 61 (2014) 1048–1055.
[4] T. Konishi, A.B. Lentsch, Hepatic ischemia/reperfusion: mechanisms of tissue injury, repair, and regeneration, Gene Expr. 17 (2017) 277–287.
[5] S. Barone, T. Okaya, S. Rudich, et al., Distinct and sequential upregulation of genes regulating cell growth and cell cycle progression during hepatic ischemia-reperfusion injury, Am. J. Physiol. Cell Physiol. 289 (2005) C826–C835.
[6] H.C. Yu, H.Y. Qin, F. He, et al., Canonical notch pathway protects hepatocytes from ischemia/reperfusion injury in mice by repressing reactive oxygen species production through JAK2/STAT3 signaling, Hepatology 54 (2011) 979–988.
[7] T. Uehara, B. Bennett, S.T. Sakata, et al., JNK mediates hepatic ischemia reperfusion injury, J. Hepatol. 42 (2005) 850–859.
[8] N. Itoh, D.M. Ornitz, Fibroblast growth factors: from molecular evolution to roles in development, metabolism and disease, J. Biochem. 149 (2011) 121–130.
[9] N. Itoh, D.M. Ornitz, Evolution of the Fgf and Fgfr gene families, Trends Genet. 20 (2004) 563–569.
[10] J. Watson, C. Francavilla, Regulation of FGF10 signaling in development and disease, Front. Genet. 9 (2018) 500.
[11] X. Zhang, O.A. Ibrahimi, S.K. Olsen, et al., Receptor specificity of the fibroblast growth factor family. The complete mammalian FGF family, J. Biol. Chem. 281 (2006) 15694–15700.
[12] N. Itoh, H. Ohta, Fgf10: a paracrine-signaling molecule in development, disease, and regenerative medicine, Curr. Mol. Med. 14 (2014) 504–509.
[13] T. Berg, C.B. Rountree, L. Lee, et al., Fibroblast growth factor 10 is critical for liver growth during embryogenesis and controls hepatoblast survival via beta-catenin activation, Hepatology 46 (2007) 1187–1197.
[14] S. Utley, D. James, N. Mavila, et al., Fibroblast growth factor signaling regulates the expansion of A6-expressing hepatocytes in association with AKT-dependent β-catenin activation, J. Hepatol. 60 (2014) 1002–1009.
[15] D.A. Fruman, H. Chiu, B.D. Hopkins, et al., The PI3K pathway in human disease, Cell 170 (2017) 605–635.
[16] B.D. Manning, A. Toker, AKT/PKB signaling: navigating the network, Cell 169 (2017) 381–405.
[17] B. Ke, X.D. Shen, Y. Zhang, et al., KEAP1-NRF2 complex in ischemia-induced hepatocellular damage of mouse liver transplants, J. Hepatol. 59 (2013) 1200–1207.
[18] O. Motiño, D.E. Francés, N. Casanova, et al., Protective role of hepatocyte cyclooxygenase-2 expression against liver ischemia-reperfusion injury in mice, Hepatology 70 (2019) 650–665.
[19] Y. Liu, T. Lu, C. Zhang, et al., Activation of YAP attenuates hepatic damage and fibrosis in liver ischemia-reperfusion injury, J. Hepatol. 71 (2019) 719–730.
[20] N. Wakabayashi, S.L. Slocum, J.J. Skoko, et al., When NRF2 talks, who's listening? Antioxidants Redox Signal. 13 (2010) 1649–1663.
[21] L. Guan, L. Zhang, Z. Gong, et al., FoxO3 inactivation promotes human cholangiocarcinoma tumorigenesis and chemoresistance through Keap1-Nrf2 signaling, Hepatology 63 (2016) 1914–1927.
[22] H.K. Bryan, A. Olayanju, C.E. Goldring, et al., The Nrf2 cell defence pathway: keap1-dependent and -independent mechanisms of regulation, Biochem. Pharmacol. 85 (2013) 705–717.
[23] X. Wu, X. Wu, Y. Ma, et al., CUG-binding protein 1 regulates HSC activation and liver fibrogenesis, Nat. Commun. 7 (2016) 13498.
[24] T. Lan, C. Li, G. Yang, et al., Sphingosine kinase 1 promotes liver fibrosis by preventing miR-19b-3p-mediated inhibition of CCR2, Hepatology 68 (2018) 1070–1086.
[25] Z.Z. Yan, Y.P. Huang, X. Wang, et al., Integrated omics reveals tollip as an regulator and therapeutic target for hepatic ischemia-reperfusion injury in mice, Hepatology 70 (2019) 1750–1769.
[26] H. Steiling, M. Mühlbauer, F. Bataille, et al., Activated hepatic stellate cells express keratinocyte growth factor in chronic liver disease, Am. J. Pathol. 165 (2004) 1233–1241.
[27] N. Nieto, S.L. Friedman, A.I. Cederbaum, Stimulation and proliferation of primary rat hepatic stellate cells by cytochrome P450 2E1-derived reactive oxygen species, Hepatology 35 (2002) 62–73.
[28] M. Kong, X. Chen, F. Lv, et al., Serum response factor (SRF) promotes ROS generation and hepatic stellate cell activation by epigenetically stimulating NCF1/2 transcription, Redox Biol. 26 (2019) 101302.
[29] C.R. Gandhi, Hepatic stellate cell activation and pro-fibrogenic signals, J. Hepatol. 67 (2017) 1104–1105.
[30] W.Z. Guo, H.B. Fang, S.L. Cao, et al., Six-transmembrane epithelial antigen of the prostate 3 deficiency in hepatocytes protects the liver against ischemia reperfusion injury by suppressing transforming growth factor-β-activated kinase 1, Hepatology 71 (2020) 1037–1054.
[31] Y.H. Li, H.L. Fu, M.L. Tian, et al., Neuron-derived FGF10 ameliorates cerebral ischemia injury via inhibiting NF-κB-dependent neuroinflammation and activating PI3K/Akt survival signaling pathway in mice, Sci. Rep. 6 (2016) 19869.
[32] X. Fang, L. Wang, L. Shi, et al., Protective effects of keratinocyte growth factor-2 on ischemia-reperfusion-induced lung injury in rats, Am. J. Respir. Cell Mol. Biol. 50 (2014) 1156–1165.
[33] X. Tan, H. Zhu, Q. Tao, et al., FGF10 protects against renal ischemia/reperfusion injury by regulating autophagy and inflammatory signaling, Front. Genet. 9 (2018) 556.
[34] T. Konishi, R.M. Schuster, A.B. Lentsch, Proliferation of hepatic stellate cells, mediated by YAP and TAZ, contributes to liver repair and regeneration after liver ischemia-reperfusion injury, Am. J. Physiol. Gastrointest. Liver Physiol. 314 (2018) G471–G482.
[35] T. Kaizu, A. Ikeda, A. Nakao, et al., Protection of transplant-induced hepatic ischemia/reperfusion injury with carbon monoxide via MEK/ERK1/2 pathway downregulation, Am. J. Physiol. Gastrointest. Liver Physiol. 294 (2008) G236–G244.
[36] T. Kong, M. Liu, B. Ji, et al., Role of the extracellular signal-regulated kinase 1/2 signaling pathway in ischemia-reperfusion injury, Front. Physiol. 10 (2019) 1038.
[37] L. Yang, W. Wang, X. Wang, et al., Creg in hepatocytes ameliorates liver ischemia/reperfusion injury in a TAK1-dependent manner in mice, Hepatology 69 (2019) 294–313.
[38] C. Schmidt, B. Peng, Z. Li, et al., Mechanisms of proinflammatory cytokine-induced biphasic NF-kappaB activation, Mol. Cell. 12 (2003) 1287–1300.
[39] A. Kulisz, N. Chen, N.S. Chandel, et al., Mitochondrial ROS initiate phosphorylation of p38 MAP kinase during hypoxia in cardiomyocytes, Am. J. Physiol. Lung Cell Mol. Physiol. 282 (2002) L1324–L1329.
[40] Y. Xin, Y. Bai, X. Jiang, et al., Sulforaphane prevents angiotensin II-induced cardiomyopathy by activation of Nrf2 via stimulating the Akt/GSK-3ß/Fyn pathway, Redox Biol. 15 (2018) 405–417.
[41] H. Hu, L. Hao, C. Tang, et al., Activation of KGFR-Akt-mTOR-Nrf2 signaling protects human retinal pigment epithelium cells from Ultra-violet, Biochem. Biophys. Res. Commun. 495 (2018) 2171–2177.
[42] A. Cuadrado, A.I. Rojo, G. Wells, et al., Therapeutic targeting of the NRF2 and KEAP1 partnership in chronic diseases, Nat. Rev. Drug Discov. 18 (2019) 295–317.
[43] A.P. Gureev, E.A. Shaforostova, V.N. Popov, Regulation of mitochondrial biogenesis as a way for active longevity: interaction between the Nrf2 and PGC-1α signaling pathways, Front. Genet. 10 (2019) 435.
[44] T.A. Beyer, W. Xu, D. Teupser, et al., Impaired liver regeneration in Nrf2 knockout mice: role of ROS-mediated insulin/IGF-1 resistance, EMBO J. 27 (2008) 212–223.

[45] N. Lehwald, G.Z. Tao, K.Y. Jang, et al., Wnt-β-catenin signaling protects against hepatic ischemia and reperfusion injury in mice, Gastroenterology 141 (2011) 707–718.
[46] N. Yang, R.I. Mahato, GFAP promoter-driven RNA interference on TGF-β1 to treat liver fibrosis, Pharm. Res. (N. Y.) 28 (2011) 752–761.
[47] S.N. Greenhalgh, K.P. Conroy, N.C. Henderson, Cre-activity in the liver: transgenic approaches to targeting hepatic nonparenchymal cells, Hepatology 61 (2015) 2091–2099.